



ENHANCED PHOTO CATALYTIC DEGRADATION OF METHYLENE BLUE DYE UNDER DIRECT SUNLIGHT BY TITANIUM DOPED TIN OXIDE NANO PARTICLES

J. R. Sheeba*¹, M. S. Anandha Prabhu¹, S. Radhika², G. Edwin Sheela¹

¹Department of Physics, Muslim Arts College, Thiruvithancode, TamilNadu, India

²Department of Physics, Pioneer Kumaraswamy College, Nagercoil, TamilNadu, India

(Affiliated to Manonmaniam Sundaranar University, Abishekapatti, Tirunelveli)

*Corresponding author: jrsheeba@rediffmail.com

Received: 04-5-2022; Revised: 06-07-2022; Accepted: 12-07-2022; Published: 31-08-2022

© Creative Commons Attribution-NonCommercial-NoDerivatives 4.0 International License <https://doi.org/10.55218/JASR.202213713>

ABSTRACT

Titanium doped nanosized tin oxide photo catalysts are synthesized for the first time using simple co-precipitation method. The degradation experiment demonstrates the synergistic effect between adsorption and photo catalysis for the removal of methylene blue (MB) under the sun light for irradiation. The prepared photo catalysts are characterized by using X-ray diffraction, SEM and EDAX, UV-Vis Spectra and photo luminescent. The crystallite size is determined from XRD analysis and is found to range from 3.81nm to 18nm. The blue shift in the UV-Vis absorbance spectra confirms the quantum confinement of the samples. The substitution of Sn by Ti in the rutile structure increases the concentration of oxygen vacancies as it enhances the degradation of methylene blue dye under direct sunlight. The maximum photo catalytic removal efficiency of the synthesized samples for methylene blue dye is 95.6% in 45min.

Keywords: Adsorption, Photo catalysis, Methylene Blue Dye, SnO₂.

1. INTRODUCTION

In the recent past, the environment pollution due to industrialization has brought a great attention towards scientific community in the area of adsorption and photo catalysis [1]. Toxic organic compounds come from various sources such as industries, households, etc. [2]. Specifically, the organic dyes are the major constituent of pollutants in wastewater released from textile, leather, cosmetics, paper, plastics, etc. [3, 4]. The general toxicity and the chemical stability of the organic dye pollutants bring harm to the ecosystem when released into the water bodies such as rivers, lakes, ponds and seas without any prior treatment. These pollutants can produce toxic products through hydrolysis, oxidation or other chemical reactions in the water bodies. Therefore, these organic dyes must be removed from the industrial wastes. The usual methods of the removal of dyes from the industrial waste are adsorption [5], biodegradation [6], chemical methods such as chlorination, ozonation [7]. These treatments of the dyes bring several problems since dyes have synthetic origin and complex aromatic molecular structures which make them very stable and generally difficult to be biodegraded and photo degraded [8].

Nowadays advanced oxidation such as Fenton oxidation [9], photo-Fenton oxidation [10, 11], and photo catalysis [12] have been used in wastewater treatment. Which among, the photo catalysis is a process by which light of appropriate wavelength is used by the catalyst which involves the transfer of electrons from the valence band to the conduction band to degrade the organic dyes into carbon di oxide and water without any other toxic products [13].

Scientists have developed many nano metal oxides such as TiO₂ [14], BiVO₄ [15], Ag₃PO₄ [16] and ZnO [17], Cu_xZn_{1-x}O composite [18], etc. and they show photo catalytic activity for organic dye degradation due to their larger surface to volume ratio. However, the practical application of photo catalysis in wastewater treatments is hampered due to its lower thermal and chemical instability, relatively higher cost of catalysts and lower efficiency of decomposition of dyes and usually suitable for the removal of dye wastewater with low concentration [19]. Among these nano metal oxides, tin oxide behaves as a promising element of photo catalyst due to their high surface reactivity, large number of active sites, and high adsorption power of light energy [20]. An effort has been taken to study the

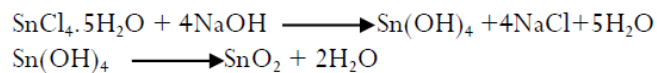
photo catalytic activity of environment friendly, chemically stable, n-type semiconductor tin oxide nano particles with a wide band gap [21] of 3.6eV. Tin oxide nano particles have a variety of applications such as optoelectronic devices, conductive electrodes [22], transparent coatings [23], dye sensitized solar cells [24], transistors [25], optical sensors [26], gas sensors [27, 28], alcohol sensors [29, 30], formaldehyde sensors [31], super capacitor applications [32, 33]. Nano tin oxide has no adverse health effects and is poorly absorbed by the human body when injected or inhaled [34]. Although pure tin oxide has good thermal and chemical stability, pure tin oxide does not show very good efficiency in photocatalytic degradation of organic dye due to its wide band gap energy and greater recombination rate of the generated electron-hole pairs [35]. Addition of transition metal ions imparts more free electrons in the case of n-type semiconductor ensuing in the narrow down of band gap [36]. As a result, irradiation of visible range of electromagnetic radiation generates excited electrons and ultimately this enhances photo catalysis. Several works have been reported on doping of tin oxide with transition metals which include gold [37], manganese [38], silver [39, 40], zinc [41], and iron [42] to enhance the photo catalytic activity. In the present work we report the adsorption and photo catalytic activity of pure and titanium doped tin oxide nano particles for the degradation of methylene blue organic dye under direct sunlight irradiation.

2. MATERIAL AND METHODS

2.1. Preparation of Tin oxide nano particle

SnO₂ samples were prepared using Tin chloride (IV) Penta hydrate (SnCl₄.5H₂O, Sigma Aldrich) as a precursor, NaOH as precipitating agent and EDTA as surfactant. 1M of Tin chloride (IV) Penta hydrate was slowly added to 50mL of de-ionized water at room temperature under constant stirring to produce a transparent colloidal solution. NaOH was added drop wise to the colloidal solution in order to modulate the pH at 3 uniformly throughout the reaction. The colloidal solution was then left for constant stirring for about 5 hours at 60°C. A white precipitate formed was obtained and filtered using Whatman filter paper and washed with de-ionized water several times until the effluent pH became neutral. At last, after washing with de-ionized water, the precipitate is washed with ethyl alcohol. After drying the precipitate was calcined at 170°C in a hot air oven for about 2 hours, the SnO₂

nano particles were obtained. The reaction mechanism in the synthesis of tin oxide nano particles is given below:



2.2. Preparation of Ti doped SnO₂ Nano Powder

For the preparation of Ti doped SnO₂ nano powder, 0.02M, 0.06M and 0.1M of TiO₂ was added to the 1M tin chloride solution and the pH was balanced as 3. The mixture was stirred constantly for 5 hours. The procedure adopted to prepare nano structured pure SnO₂ was used to obtain Ti doped SnO₂ nano particles.

2.3. Preparation of samples for photo catalytic activity

A 0.5 ml of methylene blue solution was added in 500ml of de-ionized water and dissolved. Now 0.5 gm of all the prepared pure and titanium doped tin oxide nano particles were mixed with 100ml of the above solution in four beakers separately, and the remaining 100ml MB solution was kept in a beaker. The beakers were covered well with aluminum foil in order to avoid the entering of light. The beakers with solution were stirred for 5 minutes and covered well with aluminium foil in order to avoid the entering of light. The suspension was placed in dark condition for 30 minutes to ensure an adsorption-desorption equilibrium. The samples were collected from all the four beakers for every 10 minutes. Up to 10 minutes the dye de-colorizes rapidly and there after the colour fades a little. The colour of the MB dye remains the same after 30 minutes. Since the dye stop de-colorization, the aluminium foils were removed from the beakers and placed in sunlight. The samples were collected in equal intervals of time and further investigations were performed.

3. RESULTS AND DISCUSSION

3.1. XRD Analysis

The crystallite size and phases of pure and Ti doped nano particles were determined by XRD analysis. XRD data were collected using X'Pert Pro X-ray diffractometer (CuK_α target, =1.5406 Å) in the 2theta range of 20°-80° and the diffraction pattern of pure and Ti doped SnO₂ were shown in fig. 1. The diffraction peaks were in harmony with JCPDS card no: 41-1445 and the synthesized samples show tetragonal rutile structure [43]. The cell parameters a, c and cell volume V of the synthesized samples were calculated using the formula

$$1/d_{hkl}^2 = (h^2 + k^2)/a^2 + l^2/c^2$$

Where, h, k, l were miller indices and d_{hkl} , the unit cell volume of the tetragonal system are, $V = a^2c$ [44]. The crystalline size, D, of all the samples were calculated from the peak width with the Scherrer's formula: $D = (K\lambda)/(\beta\cos\theta_B)$ where, λ - X-ray wavelength, β - full width half maximum (FWHM) of a diffraction peak, θ_B - the diffraction angle and K - the Scherrer's constant of the order of units [45, 46].

The lattice parameters, cell volume, average crystallite size, tetragonal distortion and band gap of the pure and Ti doped tin oxide nano particles were given in table 1. The lattice parameters of all the Ti doped samples vary from the pure SnO_2 and is due to the incorporation of Ti^{4+} ions into the SnO_2 crystal system since the ionic radius of Sn^{4+} and Ti^{4+} ions are 0.69Å [47] and 0.74Å [48] respectively. The crystallite size increases with the increase in the Ti ion concentration. The increase in the crystallite size is due to the incorporation of Ti^{4+} and is attributed to the creation of tin or oxygen vacancies and also leads to the assembly of bigger grains of Ti doped SnO_2 compared to pure SnO_2 respectively [49, 50]. When Ti^{4+} substitutes Sn^{4+} the lattice should expand as the size of Ti^{4+} is larger than that of Sn^{4+} [51]. Number of unit cell in the crystal is calculated using the relation,

$$n = \pi D^3 / 6V$$

where, D is the crystallite size and V is the volume of the unit cell [52]. The tetragonal distortion c/a ratio is calculated and is given in table 1.

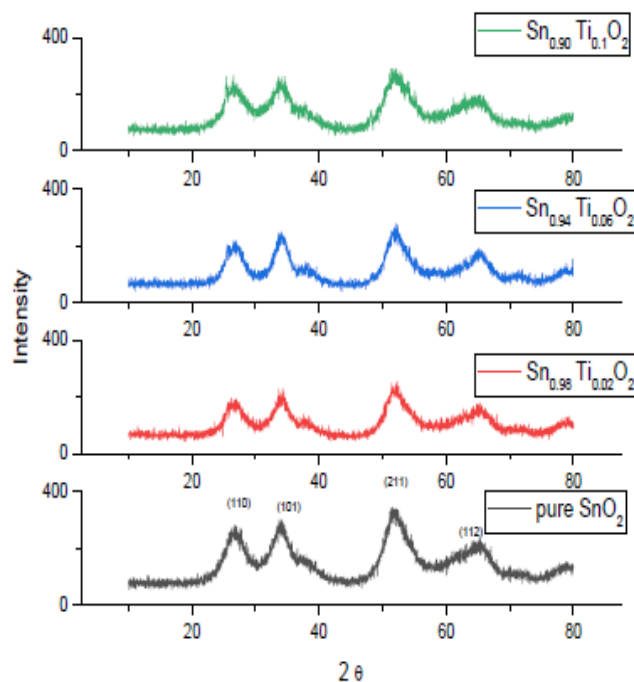


Fig. 1: XRD pattern

Table 1: Lattice parameters, crystallite size, tetragonal distortion and band gap of pure and Ti doped SnO_2

Samples	Lattice parameters		Cell Volume $V = a^2c \text{Å}^3$	Crystallite size Nm	Number of unit cell in the crystal	Tetragonal distortion c/a	Band gap Ev
	aÅ	cÅ					
Pure SnO_2	4.7059	3.1606	69.9954	3.871	433	0.6716	3.99
$\text{Sn}_{0.98}\text{Ti}_{0.02}\text{O}_2$	4.6953	3.1597	69.6626	9.87	7223	0.6729	3.232
$\text{Sn}_{0.94}\text{Ti}_{0.06}\text{O}_2$	4.7015	3.1561	69.7645	13.80	19714	0.6712	3.211
$\text{Sn}_{0.90}\text{Ti}_{0.1}\text{O}_2$	4.7367	3.1635	70.9821	18.38	45778	0.66787	3.201

3.2. SEM and EDAX Analysis

3.2.1. SEM Analysis

The morphology of pure and Ti doped SnO_2 were characterized by using Scanning Electron Microscope (SEM) CARL ZEISS EVO18 and is depicted in Fig. 2. The morphology of samples was tetragonal with one sharp corner in each particle. The sharpness diminishes with the increase in concentration and becomes almost spherical. Agglomeration of the particles was also observed. This may be due to the minimizing of the high surface and interfacial energy of particles. This study also revealed the better appearance of homogeneity in shape and size of the nanoparticles under the resolutions taken.

3.2.2. EDAX analysis

Pure and Ti doped SnO_2 nanoparticles were also subjected to examine the chemical formation and composition using EDAX analysis and is shown in fig. 3. The EDAX spectrum confirmed the presence of Sn, O and Ti elements and the atomic weight percentage of all the synthesized nano materials is given in fig. 3. The EDAX spectrum of all the samples also confirms the absence of impurities that arises from the precursor during the synthesis process. Thus, the synthesized SnO_2 nanoparticles were present in their pure forms. The steady and pointed peaks with Sn, O, and Ti demonstrated that synthesized tin oxide nano particles were crystalline in nature [53]. The crystalline nature agrees well with the XRD report.

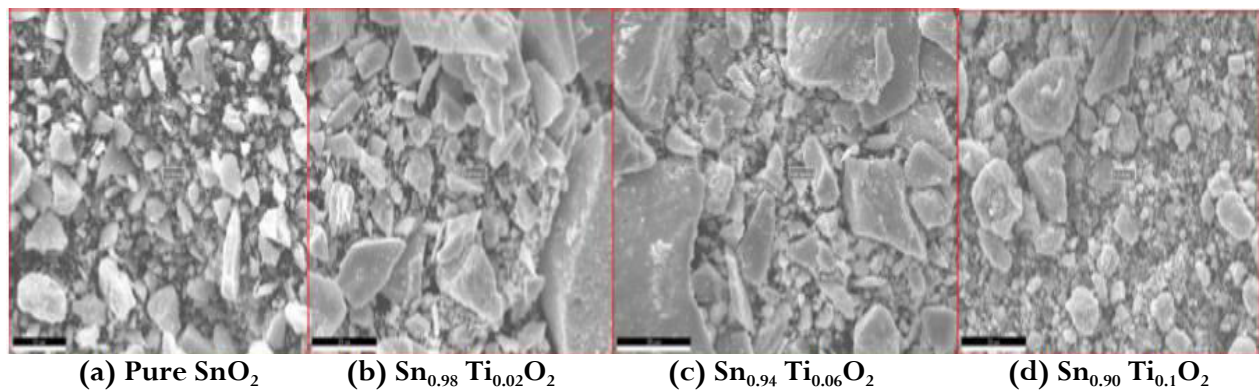


Fig. 2: SEM images of pure and titanium doped tin oxide

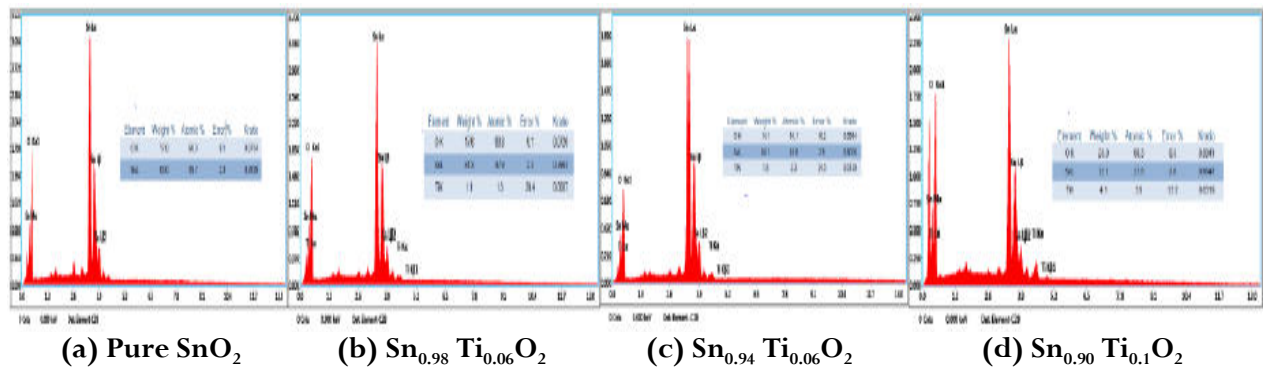


Fig. 3: EDAX images of pure and titanium doped tin oxide

3.3. UV-Visible Spectrum

An absorbance spectrum of pure SnO_2 and Ti doped SnO_2 nanocrystals were shown in fig. 4. Pure SnO_2 illustrates an absorption peak at 310 nm and the optical band gap is found to be 3.996eV using the relation $E_g = hc/\lambda$ where, h is Planck's constant, λ is the wavelength; c is the velocity of light and E_g is the optical band gap [54]. Blue shift is observed for the Ti doped nano SnO_2 .

The optical band gap of all the Ti doped samples decreases as the concentration of titanium increases and is given in table 1. The band gap energy of the electron-hole pair due to quantum confinement is inversely proportional to the radius from the following equation. Thus, as the crystallite size increases there is decrease in the band gap of the prepared samples which is shown in table 1.

$$\Delta E_g = \frac{\hbar^2 \pi^2}{2\mu R^2} - \frac{1.8e^2}{\epsilon R}$$

Where R is the particle radius, \hbar is planks constant, e is the charge of the electron, μ is the effective reduced mass, ϵ is the static dielectric constant [55].

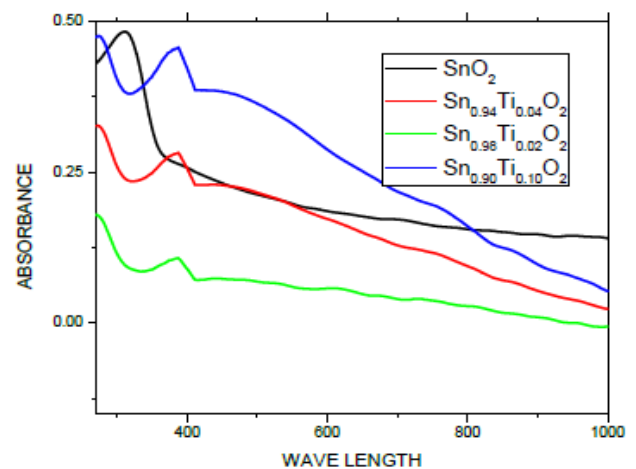


Fig. 4: UV Absorbance of pure and Ti doped SnO_2 nano particles

3.4. Photoluminescence Spectra

The photoluminescence spectroscopy is a technique to determine the crystalline quality, surface defects, energy bands and exciton fine structure of the nanocrystals. The PL spectra of the synthesized pure and Ti doped SnO_2 nano particles are shown in Fig.5. The emission peaks are at 354nm, 489nm and 536nm for

pure SnO₂ nanocrystals. The peak at 354nm is shifted to 387nm and also, there is a decrease in the intensity of the PL spectra for all the Ti doped SnO₂ nano particles. This is due to the fact that Ti⁴⁺ ion is incorporated in the SnO₂ lattice and this leads to the local disorder but also the position of oxygen as well as tin vacancies. The emission wavelength of the oxide material depends mainly on the particle shape, size, and excitation wavelength [56]. The UV peak centered at 354nm is generally ascribed to the near band edge emission from the holes in the valence band and the radioactive recombination of electrons in the conduction band. This emission peak at 354nm is due to high crystalline nature and perfect surface states [57]. The emission at 354nm equivalent to the 3.5eV energy corresponds to the de-excitation from the conduction band of Sn⁴⁺3d to the valence band of O²⁻(2p). The blue emission of SnO₂ at 489nm (2.54eV) is attributed to the emission of trapped electrons in the defect levels within the band gap, such as O vacancies and Ti interstitials formed during the process of synthesis [58, 59]. The green emission peak at 536nm (2.31eV) is attributed to deep traps forming defect energy levels inside the SnO₂ band gap of all the synthesized samples [60].

Pure and Ti doped SnO₂ nano crystals is synthesized by co-precipitation method and thus a high density of oxygen and tin vacancies is expected which is responsible for the interactions between these oxygen and interfacial tin vacancies [61]. This leads to the formation of a number of trapped states which form a series of metastable energy levels within the band gap result into a strong PL signal at room temperature. Thus, these intermediate states are responsible for the enhancement of photo catalysis activity of MB dye.

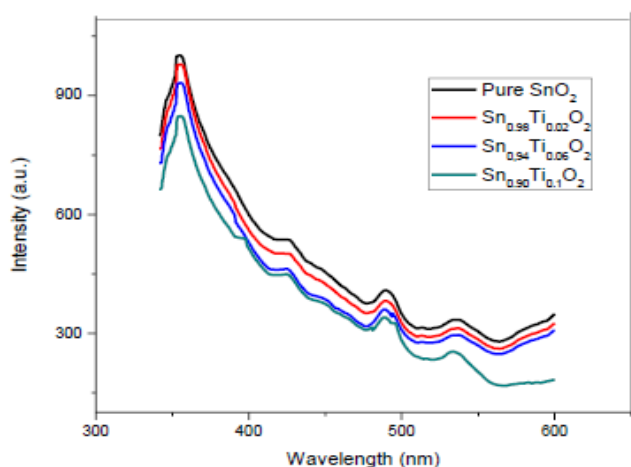


Fig. 5: PL spectra of pure and Ti doped SnO₂ nano particles

3.5. Adsorption and photo catalytic degradation of methylene blue

The steps involved in the degradation process of organic dyes are a) adsorption of reactants onto the surface, (b) reaction taking place on the surface, (c) desorption of products from the surface [62]. The surface area of nano particles is more than that of the bulk. Due to this larger surface area, the catalyst can easily adsorb on the dye molecule. In order to quantify the effect of adsorption on the degradation of methylene blue organic dye with the chemical formula (C₁₆H₁₈ClN₃S), 0.5 g of the pure and Ti doped samples are mixed with methylene blue dye in separate beaker. The pH of the solution is maintained at 7. The beaker was covered by aluminum foil to prevent the exposure of light and stirred constantly in a magnetic stirrer. The colour of the dye has not been changed when the dye is added with pure SnO₂ but the dye decolorizes when added with Ti doped SnO₂ nano crystals indicating the process of adsorption and is shown in the figure 6. The intensity of the absorption peak at 664 nm decreased significantly with increase in the doping concentration of Ti in SnO₂. These results reveal an increase in the mineralization of MB dye of tin oxide through Ti doping process. However, MB dye has not been completely decolorized and effort has been taken under sunlight irradiation for photo catalysis.

The adsorption amounts of pure and Ti doped SnO₂ nano particles are determined by recording variations in the MB-absorption band at wavelength $\lambda_{max} = 664$ nm which corresponds to the strongest absorption wavelength for MB. The percentage of degradation of the dye and quantity of the dye adsorbed were calculated by using the following equations.

$$\% \text{ Degradation} = (C_0 - C_t) / C_0 \times 100 = ((A_0 - A) / A_0) \times 100$$

The degradation of the MB dye takes place as soon as the dye is mixed with the catalyst. The MB molecules are adsorbed on the surface of Ti doped SnO₂ catalyst. This enhances the excitation of electrons to the conduction band and simultaneously increases the electron transfer to the adsorbed O₂. After 30 minutes, the degradation of the dye stops because of the saturation of adsorption of the molecules at the surface. The removal efficiency remains the same there after. The degradation efficiency are 3.61%, 14.54%, 38.71%, 49.02% for pure SnO₂ and Ti (0.02M, 0.06M, 0.1M) doped SnO₂ respectively. Now the system is irradiated with visible photons by keeping the solution in direct sunlight. The removal efficiency is increased as the dopant concentration of Ti

ion is increased in the SnO_2 lattice. The increase in the removal efficiency is influenced by factors such as morphology, crystalline nature, crystallite size, porosity and surface area [63]. The doping concentration of Ti in SnO_2 increases the crystallite size and due to quantum

confinement effect, the band gap shrinks. The smaller band gap energy due to Ti doping plays another role in enhancing the visible light photo catalytic activity of SnO_2 catalyst.

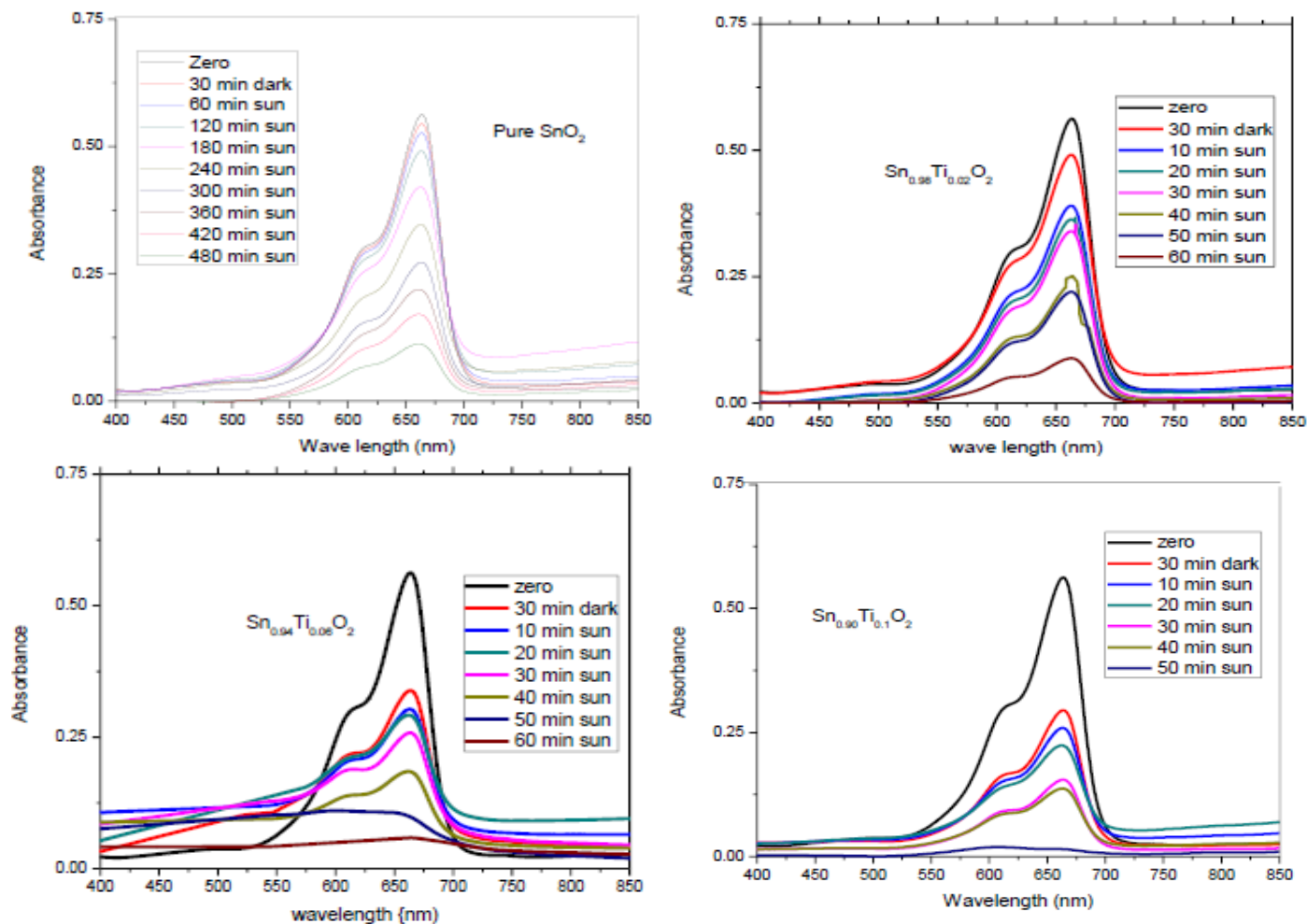


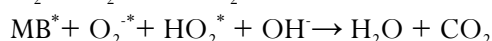
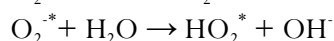
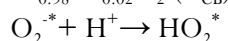
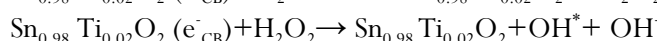
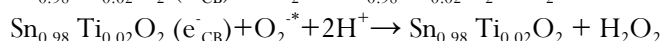
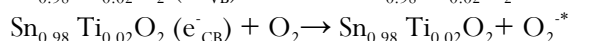
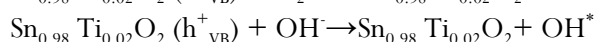
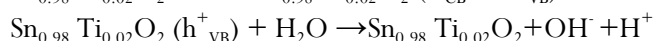
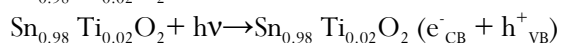
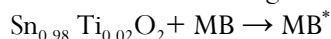
Fig. 6: UV- Visible spectra of degradation efficiency of MB dye using pure and Ti doped SnO_2

As soon as the solar light enters the dye added with photo catalyst, electrons from the valence band move to the conduction band of the tin oxide nano particles [64]. Furthermore, oxygen vacancies act as a donor with an energy level at 2.54 eV (489 nm) which is obtained from PL spectra of all the synthesized samples. Consequently, the energy position of oxygen vacancies generates the holes in the valence band under visible light irradiation.

In Ti^{4+} doped material, the Sn^{4+} lattice position is replaced by Ti^{4+} ions, this will lower the energy level of conduction band of SnO_2 . Also, it can be considered that the titanium ions have transferred their energy into the conduction band of which can act as a mediator of

interfacial charge transfer leading to light induced charge carriers [65]. The electron can excite from the valence band of Ti energy level. Then the photo generated electrons can easily move from the conduction band of Ti doping energy level to the surface of photo catalyst to capture adsorbed O_2 which improve the separation efficiency of charge carriers. These photo generated electrons are transferred from excited state of adsorbed molecules to the conduction band of nano particles thus facilitating the production of active species for photo catalysis such as hydroxyl (HO^\bullet), hydrogen peroxides (HO_2^\bullet) and superoxide ($\text{O}_2^{\bullet-}$) radicals. These active species will in turn oxidize the organic compounds adsorbed on the oxide surface and reacts at

the ortho-, para-, or meta-positions of the benzene ring depending on the nature of functional groups attached to the ring [66]. Finally, the nano sized Ti doped SnO₂ and pure SnO₂ mineralizes the MB dye into carbon dioxide, water, and inorganic nitrogen with nitrate ion gradually [67- 69]. Fig. 7 shows the degradation mechanism and the degradation reaction is given below:



The normalized residual concentration of MB dye is evaluated using

$$C_t / C_0 = A_t / A_0$$



Fig. 7: Methylene blue dye degradation mechanism

Where, C_0 and C_t are the initial and residual concentration of MB dye, A_t and A_0 are the absorbance intensity at time t and at time $t = 0$ [70]. Fig. 8 shows the plot of the ratio of C_t/C_0 vs irradiation time. The graph illustrates that there is no remarkable degradation of the dye without catalyst. But, when pure SnO₂ was added with the dye and kept in sun light 80.14% of the dye degraded in a duration time of 8 hours. When Ti (0.02M, 0.06M) doped SnO₂ is used as catalyst 84.69% and 89.54% of the dye degraded in a very short duration time of 60 minutes. Ti (0.1M) doped SnO₂ photo catalyst mineralizes 95.59% of MB dye in a duration time of 50 minutes. Hence, this dye degradation process of Ti (0.1M) doped with SnO₂ as catalyst was investigated by collecting and reusing same catalyst for

multiple cycle of MB dye degradation process and is depicted in figure 9. A small decrement in the degradation efficiency is observed after five cycles due to incomplete recollection and loss during washing. SnO₂ nano particles doped with titanium is a stable catalyst and have great potential application in waste water treatment.

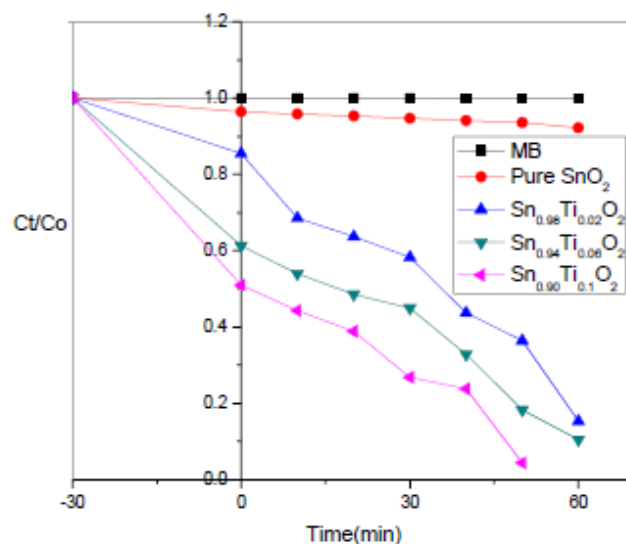


Fig. 8: MB degradation efficiency of Pure and Ti doped SnO₂

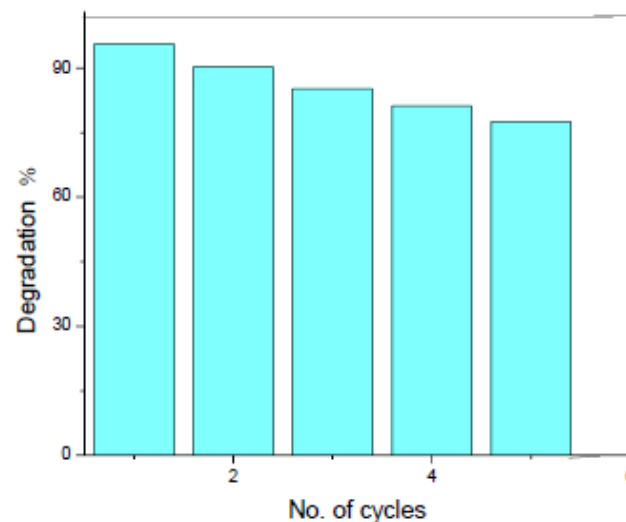


Fig. 9: MB degradation percentage of Ti (0.01M) doped SnO₂ for five cycles

4. CONCLUSION

Pure and Ti doped SnO₂ photo catalysts were prepared in nano size varying with tetragonal rutile structure from 3.871nm to 18.38nm. The synthesized nano sized samples of pure and Ti doped SnO₂ were characterized

by using XRD, SEM, EDAX, UV-Vis spectra and PL spectra. The SEM analysis depicts the tetragonal morphology and the EDAX confirms the elemental composition of the synthesized samples. The UV spectra show the blue shift and the band gap energy decreases with increase in crystallite size as dopant concentration increases. Active species such as O_2^{*-} , HO_2^* , OH^* , H_2O_2 , and HO_2^- generated during the irradiation of sun light are responsible for the degradation of methylene blue dye are formed due to the doping of titanium. From the present work, it is evident that Ti (0.1M) doped SnO_2 acts as a good photo catalyst in sunlight. The merits of low band gap and more oxygen vacancies, exhibits the highest sun-light photocatalytic activity of 95.59% of degradation of MB dye. Very good photo stability and recyclability was accomplished under sun-light irradiation for Ti (0.1M) doped SnO_2 . The synergistic effect of both adsorption and photo catalysis demonstrates the degradation of methylene blue dye in both dark as well as direct sun light. Thus, the synthesized samples are found to be good in waste water treatment of organic effluents of industrial waste.

Conflict of interest

All the work was carried out by the authors. The authors declare that there is no personal or financial relationship that can be viewed as potential conflicts of interest about the publication on the manuscript file. The authors had not received any source of funding.

5. REFERENCES

- Linares N, Silvestre-Albero AM, Serrano E, Silvestre-Albero J, Garc'ia-Mart'inez J. *Chemical Society Reviews*, 2014; **43(22)**:7681–7717.
- Phipps GL, Holcombe GW, Fiandt JT, *Bull. Environ. Contam. Toxicol*, 1981; **26**:585–593.
- Chowdhury S, Balasubramanian R. *Appl. Catal. B: Environ*, 2014; **160–161**:307–324.
- Martinez-Huitle CA, Brillas E. *Appl. Catal. B: Environ*, 2009; **87**:105–145.
- Gupta V. *J. Environm. Manag.*, 2009; **90(8)**:2313–2342.
- Lorenc-Grabowska E, Gryglewicz G, *Dyes Pigments*, 2007; **74(1)**:34–40.
- Moussavi G, Mahmoudi M, *Chem. Eng.*, 2009; **152**: 1–7.
- Muruganandham M, Swaminathan M. *Dyes and Pigments*, 2006; **68**:133–142.
- Sun JH, Sun SP, Wang GL, Qiao LP. *Dyes Pigments*, 2007; **74**:647–652.
- Elmorsi TM, Riyad YM, Mohamed ZH, Abid HMM, and Bary E. *Journal of Hazardous Materials*, 2010; **174**:352–356.
- Xie YB and Li XZ. *Materials Chemistry and Physics*, 2006; **95**:39–50.
- Alnuaimi MM, Rauf MA, Ashraf SS. *Dyes Pigments*, 2007; **72**:367–371.
- Seftel EM, Popovici E, Mertens M, DeWitte K, Van Tendeloo G, Cool P, Vansant EF. *Microporous Mesoporous Mater*, 2008; **113**:296–304.
- Han F, Kambala VSR, Srinivasan M, Rajarathnam D, Naidu R. *Appl. Catal.*, 2009; **359**: 25–40.
- Obregon S, Caballero A, Colon G. *Appl. Catal.*, 2012; **117**:59–66.
- Yi Z, Ye Z, Kikugawa N, Kako T, Ouyang S, Stuart-Williams H, Yang H, Cao J, Luo W, Li Z, Liu Y, Withers RL. *Nat. Mater*, 2010; **9**:559–564.
- Yu J, Yu X. *Environ. Sci. Technol.*, 2008; **42**:4902–4907.
- Sugi S, Rajalakshmi PU, Shanthi J, *Optik*, 2017; **131**:406–413.
- Wang S, Guan Y, Wang L, Zhao W, He H, Xiao J, Yang S, Sun C, *Appl. Catal.*, 2015; **168**:448–457.
- Sadeghzadeh-Attar, *Solar Energy Materials and Solar Cells*, 2018; **183**:16–24.
- Yeow SC, Ong WL, Wong ASW, Ho GW. *Sens. Actuators B*, 2009; **143**:295–301.
- Mathur S, Barth S, Shen H, Pyun JC and Werner U, *Small*, 2005; **1**:713–717.
- Yanhong Li, Min Shi, Meiri Wang, Jing Li, Yuanyuan Liu, Hongtao Cui, *J. Sol-Gel Sci. Techno.*, 2018; **86(2)**: 423–430.
- Ferrere S, Zaban A and Gregg BA, *J. Phys. Chem. B*, 1997; **101**:4490–4493.
- Jung CH, Lee JY, Pu LS, Lee KS and Yoon DH. *Thin Solid Films*, 2012; **520**:4726–4729.
- Sirbulu DJ, Tao A, Law M and Fan R, *Adv. Mater.*, 2007; **19**:61–66.
- Kolmakov A, Klenov DO, Lilach Y, Stemmer S and Moskovits M. *Nano Lett.*, 2005; **5**:667–673.
- Gyger F, Hubner M, Feldmann C, Barsan N and Weimar U, *Chem. Mater.*, 2010; **22**:4821.
- Mishra RK, Sahay PP. *Synthesis. Int.*, 2012; **38**:2295–2304.
- Varghese OK, Malhotra LK, Sharma GL. *Sens. Actuators B*, 1999; **55**:161–165.
- Zhang L, Zhao J, Zheng J, Li L, Zhu Z. *Appl. Surf. Sci.*, 2011; **258**: 711–718.
- Lim SP, Huanga NM, Lim HN. *Ceram. Int.* 2013; **39(6)**:6647–6655.

33. Murugana A, Siva V, Shameema A, AsathBahadura S, Sasikumara S, Nallamuthu N. *Journal of Energy Storage*, 2020; **28**:101194.
34. Bhattacharjee A, Ahmaruzzaman M. *RSC Adv.*, 2020; **5**:66122–66133.
35. Prakash K, Senthil kumar P, Pandiaraj S, Saravanakumar K and Karuthapandian S. *J.experimental nanoscience*, 2016; **11(14)** :1138-1155.
36. Kim DH, Lee GW, Kim YC. *Solid State Commun.* 2012; **152**: 1711–1714.
37. You H, Liu R, Liang C, Yang S, Wang F, Lu X, Ding B. *J. Mater. Chem.*, 2013; **A1**:4097–4104.
38. Anandan K, Rajendran V. *Superlattices Microstruct.*, 2015; **85**:185–197.
39. Ansari SA, Khan MM, Ansari MO, Lee J, Cho MH. *RSC Adv.*, 2014; **4**:26013–26021.
40. Saravanakumar K and Muthuraj V, *Optik*, 2017.
41. Huang H, Tian S, Xu J, Xie Z, Zeng D, Chen D, Shen G. *Nanotechnology*, 2012; **23**:105502.
42. Xia H, Zhuang H, Zhang T, Xiao D. *Mater. Lett.*, 2008; **62**:1126–1128.
43. Nehru LC, Swaminathan V, Sanjeeviraja C. *J.American of Materials Science*, 2012; **2(2)**:6-10.
44. Cullity BD, Elements of X-ray Diffraction. (Addison–Wesley, New York, 1978).
45. Pawan Chetri, Amarjyoti Choudhury. *Physica E*, 2013; **47**:257–263
46. James R Connoly. *Spring EPS*, 2007; **400**:002.
47. Ke C, Zhu W, Pan JS, Yang Z. *Current Applied Physics*, 2011; **11**:S306.
48. De-En Gu, Bang-Chao Yang, Yong-Da Hu. *Catalysis Communications*, 2008; **9**:1472–1479.
49. Riad AS, Mahmoud SA, Ibrahim AA. *Physica B: Condensed Matter*, 2001; **296(4)**:319–325.
50. Ribeiro C, Lee EJH, Giraldo TR, Longo E, Varela JA, Leite ER, *J. Phys. Chem. B* ,2004; **108**:15612.
51. Van Komen C, Punnoose A, Seehra MS. *Solid State Communications*, 2009; **149**:2257-2259.
52. NM. Shaalan, D Hamad, AY Latief, Abdel-Rahim MA. *Progress in Natural Science: Materials International*, 2016; **26**:145–151.
53. Qamara MA, Shahida S, Khana SA, Zamanb S, Sarwarb MN. *Digest Journal of Nanomaterials and Biostructures*, 2017; **12(4)**:1127 – 1135.
54. Takagahara T, Takeda K. *Phys. Rev.B.*, 1992; **461**:5578.
55. Choi WK, Jung HJ, Koh SK. *J. Vac. Sci. Technol. A Vac. Surf. Films*, 1996; **14**: 359–366.
56. Chetri P, Saikia B, Choudhury A. *J. Appl. Phys.*, 2013; **113**:233514–233522.
57. Huang MH, Wu Y, Feick H, Tran N, Weber E, Yang P. *Advan Mater.*, 2001; **13**:113.
58. Trani F, Causa M, Ninno D, Cantele G, Barone V. *Rev. B*, 2008; **77**:245410 .
59. Shajira PS, Junaid Bushiri M, Nair BB, Prabhu VG . *J. Lumin.*, 2014; **145**:425.
60. Mishra RK, Ajay Kushwaha, Sahay P.P. *RSC Adv.*, 2014; **4**:3904.
61. Gu F, Wang SF, Song CF, Lu MK, Qi YX, Zhou GJ, Xu D, Yuan DR, *Chemical Physics Letters* ,2003; **372** :451.
62. Pirkanniemi K, Sillanpaa M. *Chemosphere*, 2002; **48**:1047.
63. Yen Tsai C, Wuing Liu C, Fan C, Cheng His H, Yu Chang T. *J. Phys. Chem.*, 2017; **121**:6050–6059.
64. Kansal SK, Singh M, Sud D. *Journal of Hazardous Materials*, 2007; **141(3)**:581–590.
65. Kong XB, Li F, Qi ZN, Qi L, Yao MM. *J. Mater. Sci.: Mater. Electron.*, 2017; **28** :7660–7667.
66. Houas A, Lachheb H, Ksibi M, Elaloui E, Guillard C, Marie Herrmann J. *Appl. Catal. B Environ.*, 2001; **31**:145–157.
67. Ishibashi K, Fujishima A, Watanabe T, Hashimoto K. *J.Photochem. Photobiol A* , 2000; **134**:139.
68. Pham Van Viet, CaoMinhThi, and Le Van Hieu, *Journal of Nanomaterials*, 2016.
69. Mohammed Harshulkhan S, Janaki K, Velraj G, Sakthi Ganapthny R, Nagarajan M, *J Mater Sci: Mater Electron* ,2016 ; **27**:4744–4751.
70. Kumar S, Ojha AK. *J. Alloy. Comp.*, 2015; **644**:654-662.